Structurally complex sea grass obstructs the sixth sense of a specialized avian molluscivore

Jimmy de Fouw [a, *], Tjisse van der Heide [b, c], Thomas Oudman [a], Leo R. M. Maas [d], Theunis Piersma [a, e], Jan A. van Gils [a]

[a] Department of Coastal Systems, NIOZ Royal Netherlands Institute for Sea Research, and Utrecht University, Den Burg (Texel), The Netherlands
[b] Groningen Institute for Evolutionary Life Sciences (GELIFES), University of Groningen, Groningen, The Netherlands
[c] Aquatic Ecology and Environmental Biology Group, Institute for Water and Wetland Research, Radboud University Nijmegen, Nijmegen, The Netherlands
[d] Department of Physical Oceanography, NIOZ Royal Netherlands Institute for Sea Research, and Utrecht University, Den Burg (Texel), The Netherlands
[e] Chair in Global Flyway Ecology, Conservation Ecology Group, Groningen Institute for Evolutionary Life Sciences (GELIFES), University of Groningen, Groningen, The Netherlands

ARTICLE INFO

Predators have evolved many different ways to detect hidden prey by using advanced sensory organs. However, in some environmental contexts sensory information may be obscured. The relation between sensory organs, obstruction and searching efficiency remains little explored. In this study we experimentally examined the ways in which a sensory system ('remote detection'), which enables red knots, Calidris canutus, to detect hard objects buried in wet soft sediments, is obstructed by plants. At an important coastal nonbreeding site of this species, the Banc d'Arguin (Mauritania, West Africa), most of the intertidal foraging area is covered by sea grass. The structurally complex networks of belowground roots and rhizomes and aboveground sea grass may obstruct information on the presence of buried bivalves and thus affect searching efficiency. Under aviary conditions we offered red knots buried bivalves in either bare soft sediments or in sea grass patches and measured prey encounter rates. Red knots detected prey by direct touch in sea grass but remotely in bare sediment. Physical modelling of the pressure field build-up around a probing bill showed that within a layer of sea grass rhizomes, permeability is reduced to the extent that the pressure field no longer reveals the presence of an object. In bare sediment, where searching efficiency is constant, red knot intake rate levelled off with increasing prey density (described by a so-called type II functional response). In the sea grass beds, however, prey density increases with sea grass density and simultaneously decreases searching efficiency, which will at some point lead to a decrease in intake rate when prey densities increase (i.e. a type IV functional response). Clearly, prey detection mechanisms dictate that the combined effects of prey density and habitat complexity should be taken into account when predicting forager distributions and habitat preference.

Insights into the morphology and functionality of sensory organs in animals have contributed to our basic understanding of habitat selection and foraging distribution of animals searching for prey (Cunningham et al., 2010; Miller & Surlykke, 2001; Piersma, 2012; Sleep & Brigham, 2003). Predators have evolved multiple ways to detect their prey other than by sight. For example, bats detect their prey in the dark by ultrasonic signalling (Schnitzler & Kalko, 2001), owls use high acoustic sensitivity to detect their prey by sound in the dark (Martin, 1986) and cetacean species often use echolocation to detect their prey in the water column (Au, Benoit-Bird, & Kastelein, 2007; Madsen, Kerr, & Payne, 2004). Using their sensitive bill tip, shorebirds (Scolopacidae) have evolved a variety of ways to detect prey buried out of sight in soft sediments, including smell, taste, detection of prey vibrations, direct touch and even 'remote detection' (Gerritsen & Meiboom, 1986; Hulscher, 1982; Nebel, Jackson, & Elner, 2005; Piersma, van Aelst, Kurk, Berkhoudt, & Maas, 1998).

In some environmental contexts, sensory information may be obscured. For example, vegetation cover on the water surface obstructs echolocation-based prey detection in insectivorous bats

* Correspondence: J. de Fouw, Department of Coastal Systems, NIOZ Royal Netherlands Institute for Sea Research, and Utrecht University, P.O. Box 59, 1790 AB Den Burg (Texel), The Netherlands.
E-mail address: jimdefouw@gmail.com (J. de Fouw).

(Boonman, Boonman, Bretschneider, & van de Grind, 1998), and underwater sea grass meadows may serve as an acoustic refuge for fish from echolocation sounding by dolphins (Wilson, Wilson, Greene, & Dunton, 2013). Yet, the relation between sensory organs, obstruction and searching efficiency remains little explored (Piersma, 2011). In this study we experimentally examined whether sea grasses can obstruct prey detection by red knots, *Calidris canutus*. Red knots are highly specialized molluscivorous birds that usually forage on bivalves buried in the soft sediments of intertidal mudflats (Piersma, 2007, 2012). They have a sensory organ in the tip of the bill to detect hard-shelled prey buried in soft wet sediments without direct contact (Piersma et al., 1998). As is the case for other shorebirds, the tip of the bill contains numerous tiny pits with clusters of Herbst corpuscles, which in red knots enable the detection of self-induced pressure differences during repeated probing in wet soft sediments. Using this form of 'remote prey detection', red knots detect buried prey faster and more efficiently than if they had to rely on direct touch (Piersma et al., 1998; Piersma, van Gils, de Goeij, & van der Meer, 1995). A similar mode of prey detection has been described for kiwis (Apterygidae) and ibises (Threskiornithinae) (Cunningham et al., 2010; Cunningham, Castro, & Alley, 2007; Cunningham, Castro, & Potter, 2009).

This model of prey detection is applicable to red knots foraging on hard-shelled prey in bare soft sediments (van Gils, Spaans, Dekinga, & Piersma, 2006; Piersma et al., 1995). However, at Banc d'Arguin (Mauritania, West Africa), the subspecies *C. c. canutus* mostly encounters and uses sea grass habitats (Altenburg, Engelmoer, Mes, & Piersma, 1982; van Gils et al., 2015). These habitats consist of structurally complex networks of belowground roots and rhizomes and aboveground leaves (Larkum, Orth, & Duarte, 2006). We hypothesized that searching efficiency, i.e. the standardized rate at which foragers encounter their prey (Holling, 1959), will be negatively influenced by these structures, because the remote detection system requires unobstructed passage of water between the sediment particles (Piersma et al., 1998). To test this idea, we measured searching efficiency in red knots by offering them buried prey either in bare sediment or in sea grass-covered sediment. Here, the bare sediment treatment served as a control to verify whether red knots were able to find prey remotely (Piersma et al., 1998). Additionally, we developed a model to show the obstructing effect of sea grass rhizomes on the pressure field build-up by the probing bill. We briefly discuss the implications of this effect on the predicted relationship between prey density and intake rate (i.e. the functional response).

METHODS

Birds

The experiment was conducted in January 2011 at the research station of the Parc National du Banc d'Arguin, Mauritania, West Africa (19°53′N, 16°17′W). Six red knots were caught with mist nets on a nearby shoreline high-tide roost and colour-ringed for individual identification. All birds were successfully released after the experiments. Average bill length was 35.1 mm (range 33.6—37.0 mm) and body mass just after catching was 129 g (range 118—144 g). Birds were kept as a group in a small aviary (2.0 × 0.6 m and 0.4 m high) with sand on the floor, freshwater ad libitum, and with local natural daylight cycles and temperatures (varying between 18 and 24 °C). Every morning, the birds were weighed and their health status assessed. Birds were fed commercial trout feed (Trouvit; Skretting, Stavanger, Norway) and live bivalves that were collected locally on a daily basis. To keep birds motivated to feed during the trials, daily portions were adjusted to

keep body mass just above 100 g (e.g. van Gils & Ahmedou Salem, 2015; Oudman et al., 2014).

Experimental Design

Feeding trials were conducted in the housing cage, in which a feeding patch (10 cm depth and 15 cm radius) was created with either bare sediment or sea grass (Fig. 1c—e). *Loripes lucinalis* (8.5—10.5 mm length), the most common bivalve in our study area (Honkoop, Berghuis, Holthuijsen, Lavaleye, & Piersma, 2008), was used as prey. Per patch, either 20 or 40 prey items were offered (283 and 566 individuals/m²). All prey were buried at a fixed depth at either 1, 2 or 3 cm. For practical reasons all trials of each combination were offered in the same patch in which prey items were replaced after each trial. All density and depth combinations were offered twice to each bird (although never on the same day). Densities and depths of bivalve prey were well within the range reported for the field (Ahmedou Salem, van der Geest, Piersma, Saoud, & van Gils, 2014; van der Geest, van Gils, van der Meer, Olff, & Piersma, 2011; van Gils et al., 2015; van Gils et al., 2013; Piersma, de Goeij, & Tulp, 1993). Patches were filled with sand (mean medium grain size ± SE ($N = 6$): 248.0 ± 2.7 μm) collected at the nearby intertidal beach (19°53.026′N, 16°17.573′W). Penetrability of the sea water-saturated sand was kept constant by adding sea water until 2 mm of water remained on top of the surface.

Sea grass was collected on a tidal flat (19°53.051′N, 16°17.367′W) 500 m east of the field station. Sea grass densities were within the range reported from the field (range 2200—13 000 shoots/m²; van Lent, Nienhuis, & Verschuure, 1991; Vermaat et al., 1993). A 15 cm high sharpened PVC ring (15 cm radius) was pushed gently into the sea grass (mean shoot density ± SE ($N = 5$): 8842 ± 700 per m²). The ring with the sea grass bed was taken out. Metal pins were pushed in horizontally from the side of the ring through the sea grass rhizome mat forming a 2.5 × 2.5 cm mesh holding the sea grass mat intact. Next, the sediment was carefully sieved out, a time-consuming process that was needed to remove all prey living in the sea grass in order to be able to offer precise experimental prey densities. Eventually, a 'clean' intact sea grass mat (rhizomes, roots and leaves) remained in the ring, which was then placed in a 15 cm radius, 10 cm high container, thereafter filled with wet sand, after removing the metal pins. Next, a plastic rod with a scale was used to insert prey in their natural position into the sediment at the aimed depth, at random spatial positions. The hole was filled and the sand was smoothed (Piersma et al., 1995, 1998).

After a trial ended, the remaining prey items were counted. We never noticed prey movements or any other signs of their presence (i.e. the bivalves showing a siphon or extending a foot). Each trial was conducted with one bird at a time, with each bird being involved in at least one trial per day. Within each combination offered on a given day, the order of the birds in the trials was randomly chosen by rolling a dice. The five remaining birds were held in a separate part of the cage such that they were in vocal and visual contact with the experimental bird. A trial stopped after six prey items were encountered or after 15 min.

Searching Efficiency and Touch Model

A digital video camera (CANON Powershot G9) recorded each trial. Timing of prey encounters and ingestions were scored digitally with Etholog (Ottoni, 2000), and the recordings were played back in slow motion to confirm that we had not missed a prey encounter. In a randomly searching forager, the interval between two prey encounters, search time (T_s), is inversely related to the product of searching efficiency (a) and current prey density (D;
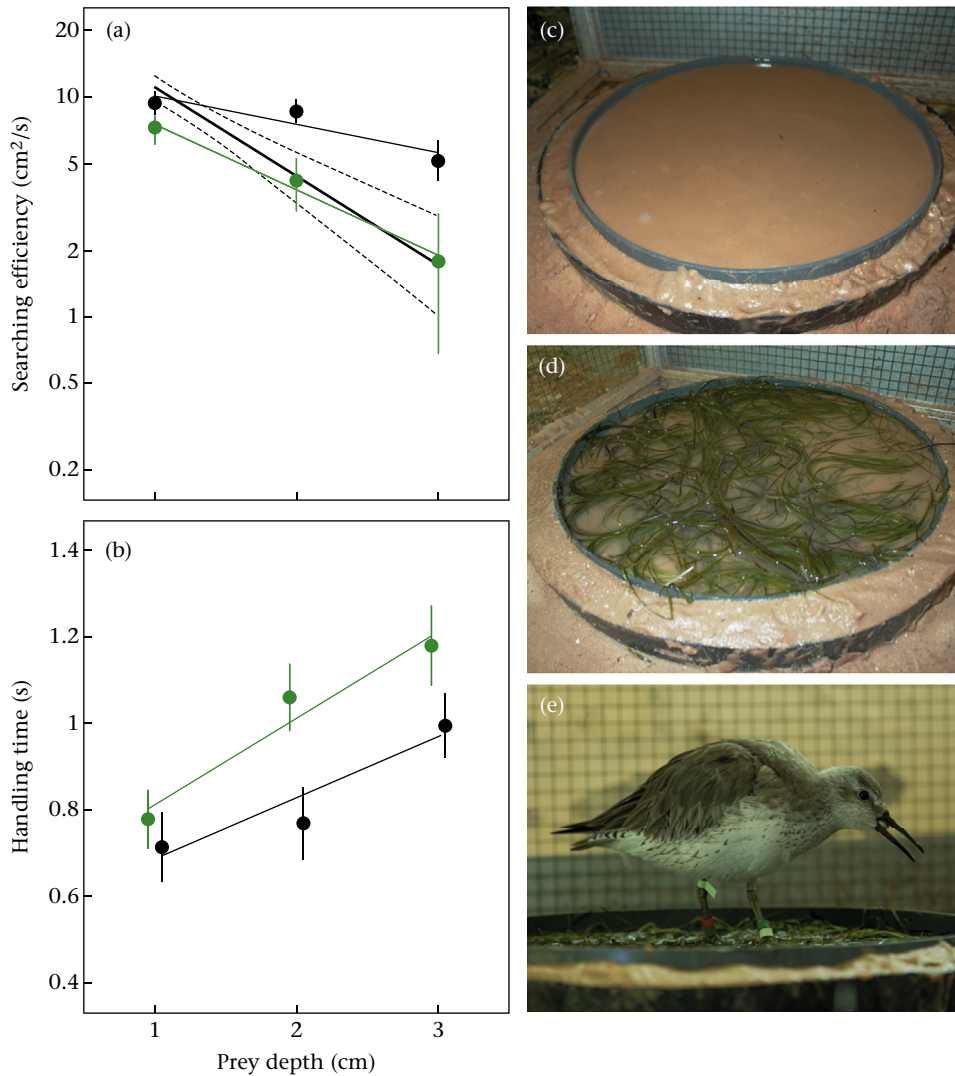
Figure 1. (a) Searching efficiency as a function of prey depth of knots foraging on prey in bare (black) and sea grass (green) habitat. The grey lines indicate the touch model with confidence interval (95%). (b) Prey handling time as a function of prey depth of knots foraging on prey in bare (black) and sea grass (green) habitat. (c) Bare patch, (d) sea grass patch, (e) knot swallowing a prey during an experimental trial on a sea grass patch.

initial prey density minus the number of prey removed; van Gils, Schenk, Bos, & Piersma, 2003):

$$\frac{1}{T_s} = aD \tag{1}$$

which can be rewritten as:

$$\log(T_s) = -\log(a) - \log(D) \tag{2}$$

In this relationship, a slope of -1 thus indicates random search, while the intercept, $-\log(a)$, reflects the negative of searching efficiency (van Gils & Piersma, 2004; Piersma et al., 1995). A searching efficiency that does not vary with prey density, together with a handling time that is constant across prey densities, leads to Holling's type II functional response (Holling, 1959). In this well-known equation, the intake rate of a forager increases as a function of prey density, initially at a rate given by searching efficiency until it levels off due to the handling time constraint. Hence, when red knots use remote prey detection the functional response has a steeper slope than with direct touch (Piersma et al., 1995).

To test to what extent red knots remotely detect buried prey, we compared the experimentally observed searching efficiency with the calculated searching efficiency based on a direct touch model (see for details Hulscher, 1982; Piersma et al., 1995; Zwarts & Blomert, 1992). We predicted a strong relation with prey depth for the observed searching efficiencies in sea grass, following the touch model (Piersma et al., 1995). The touch model was determined with the touch area of the prey (surface projection of prey area), enlarged by the surface area of the bill tip multiplied by the probe rate at each depth (1 cm classes; Appendix 1; Zwarts & Blomert, 1992). Probe rates were scored during five time intervals (ca. 10 s) for a selection of trials (all six birds equally distributed over the two habitat treatments and three prey depths, $N = 36$), by slowing down digital video recordings (1/8th of the recording speed). Probe depth was measured five times in each interval by freezing the digital video image at a probe's maximum depth and using an individual's bill length as a reference.

Statistics

Average search and handling times (each denoted by Y_i) were calculated for every trial, with individual bird as a random effect (bird$_i$):

$$\log(Y_i) = \alpha + \beta_1 \text{ prey depth}_i + \beta_2 \log(\text{prey density}_i) + \text{habitat}_i$$
$$+ \text{bird}_i + \varepsilon_i$$

where $\varepsilon_i \sim N(0, \sigma^2)$.

Search and handling times were log-transformed to meet model assumptions (when Holling's type II functional response holds then the predicted values for β_2 are -1 and 0 for search time and handling time, respectively). We used a one-sample t test for a difference between the observed and the estimated (touch-model) searching efficiency. All statistical analyses were done in R (package nlme for mixed-effect models; R Development Core Team, 2014).

The Physical Model

We developed a physical model to get mechanistic insight into how sea grass may obstruct the remote detection of red knots (for mathematical descriptions see Appendix 2). Observations and experiments by Piersma et al. (1998) showed that knots are able to remotely sense the presence of shells in wet bare sediment, and that their sensory capacity fails in dry but also in very liquid mud. However, a belowground sea grass mat, consisting of a network of roots and rhizomes, reduces the sediment layer's permeability. This may reduce the effective porosity of the soil and obstructs the pressure field built up by the probing bill of red knots. We consider first the response to a shell in a mud layer without a rhizome mat, qualitatively discussed in Piersma et al. (1998), and second, the response to a shell buried in the lower layer containing the rhizome mat.

The probing of the bill will produce pressure variations in wet sediment (pore size 180 μm). Red knots rapidly probe in the sediment over a depth of about 0.5–1 cm, usually in series of five to 10 probes at a rate of about 6–9 Hz (Piersma et al., 1998). The property of the medium at hand determines in what way it responds to pressure variations. In dry sediments it can either be supported by normal stresses (pressure) in the rigid sediment structure or be released instantaneously when it surpasses a certain threshold. In fluids, on the other hand, the pressure cannot be built up, as it will immediately respond by means of flows and waves on the water surface that will quickly remove the added energy towards infinity (see Appendix 2). In wet sediment, however, there is enough water in the pores to produce a flow through it driven by pressure differences. But as the pores are tiny channels whose sides exert a drag on the flow along them, this local increase in pressure needs time to relax and can be maintained for a while, which is the property employed by the birds.

The classical description of flow through wet sediment is one in which the pressure gradient is balanced by friction, proportional to the flow velocity. Because of the complexity of the sand skeleton this is necessarily an empirical relation, known as Darcy's law (e.g. Sleath, 1984). Since the fluid is nearly incompressible, this implies the pressure field is governed by a Poisson equation (Lamb, 1932; for details see Appendix 2).

The knot's sense of remote prey detection involves repetitive, shallow probing, followed by a single deep probe in another direction, apparently used to build up residual pressure near the bill tip. Very likely, compaction is of dominating influence. This refers to the continuous increase in residual pore pressure, owing to the 'shaking' of the muddy sand by the probing action of the bill, which may lead to a (local) compaction of sediment due to a rearrangement of sand grains in closer packing and an associated increase in pore pressure. This process plays a dominant role in liquefaction and the formation of quick sand (Sleath, 1984). For knots, the important aspects of this are that the residual (i.e. time-averaged) pressure pattern is affected by the presence of a shell and that this pattern becomes increasingly 'visible' due to its increase at each successive cycle of the probing motion. Together with the directionality offered by the set of pressure sensors (Herbst corpuscles), present over the whole circumference of the bill, this should offer the knot the ability to sense both prey direction and distance (for details see Appendix 2).

For knots foraging in sea grass, however, the permeability of the lower rhizome layer will be less than that of the upper mud layer. This is due to the decrease in the effective porosity of the sediment. We assume that the rhizome root structure is so small that we can represent its presence in the form of a reduced effective permeability which will affect the radial pressure distribution discussed above. For simplicity, we assume the permeability to be constant within the rhizome layer. Hence the pressure will again be inversely proportional to radial distance, but with reduced 'transmitted' amplitude. In fact, the semipermeable interface between the mud and rhizome layers acts as a partial mirror. This will result in an augmented pressure field in the upper sediment layer.

Ethical Note

All possible efforts were made to minimize physical and mental impact on the experimental animals. Each bird was weighed and visually inspected for general condition daily. All experimental animals were released in the wild in healthy condition after the experiment with an average body mass of 147 g (range 136–160 g) after 2 days of ad libitum food. The experiment was performed under full permission by the authorities of the Parc National du Banc d'Arguin. No animal experimentation ethics guidelines exist in Mauritania but the experiments were performed in accordance with Dutch animal experimentation guidelines. The NIOZ Royal Netherlands Institute for Sea Research has been licensed by the Dutch Ministry of Health to perform animal experiments under licence number 80200.

RESULTS

Searching Efficiency and Holling's Type II Functional Response

Search time decreased with increasing prey density with an estimated slope of -0.947 (95% confidence interval: -1.172 to -0.722) which did not differ from -1 (i.e. random search), showing that searching efficiency was independent of prey density (Table 1). Likewise, handling time was independent of prey density (Table 1). Thus, both assumptions of Holling's type II equation were met. Searching efficiency differed significantly between bare sediment and sea grass and decreased with depth (Table 1) in both habitat treatments, with the decrease being stronger in sea grass than in bare sediment (significant interaction between depth and habitat treatments: Table 1, Fig. 1a). Handling time increased significantly with prey depth in both habitat treatments and was higher in the sea grass (1.01 ± 0.05 s; mean $\pm$ SE) than in the bare patches (0.82 ± 0.05 s; Table 1, Fig. 1b).

Touch Model

There was a significant effect of depth on the probe rate (Table 2), but no effect of habitat treatment (bare sediment versus sea grass) or prey density (Table 2). In bare sediment, there was a significant difference between the predicted searching efficiency based on the touch model and the observations (Fig. 1a; at 1 cm: difference$_{observed-predicted} = -1.58$ cm^2/s, $t_{23} = -2.98$, $P < 0.01$; at 2 cm: 4.30 cm^2/s, $t_{24} = 5.98$, $P < 0.001$; at 3 cm: 3.52 cm^2/s, $t_{23} = 11.22$, $P < 0.001$). In sea grass, however, the predicted

Table 1
Mixed-effect models: test statistics and parameter estimations

	Estimate	SE	t	P
Search time (s)				
Fixed effects				
Intercept	−0.983	0.172	−5.725	<0.0001
Prey depth (1, 2, 3 cm)	0.135	0.030	4.535	<0.0001
Habitat (sea grass)	−0.024	0.091	−0.261	0.773
Prey density	−0.945	0.114	−8.320	<0.0001
Habitat∗prey depth	0.170	0.042	4.053	<0.001
Random effects				
Individual bird	1.20×10^{-5}	(SD)		
Residual	0.202	(SD)		
Searching efficiency (cm^2/s)				
Fixed effects				
Intercept	1.111	0.065	16.961	<0.0001
Prey depth (1, 2, 3 cm)	−0.135	0.030	−4.517	<0.0001
Habitat (sea grass)	0.026	0.091	0.290	0.773
Habitat∗prey depth	−0.172	0.042	−4.061	<0.001
Random effects				
Individual bird	0.015	(SD)		
Residual	0.209	(SD)		
Handling time (s)				
Fixed effects				
Intercept	−0.351	0.065	−5.388	<0.0001
Prey depth (1, 2, 3 cm)	0.095	0.016	5.872	<0.0001
Habitat (sea grass)	0.097	0.049	1.984	<0.05
Prey density	−0.001	0.001	−1.373	0.172
Habitat∗prey depth	0.001	0.022	0.011	0.992
Random effects				
Individual bird	0.135	(SD)		
Residual	0.111	(SD)		

Mixed-effect model of the log-transformed search time, searching efficiency and handling time. Models include fixed effects prey depth (continuous), prey density (continuous), habitat (categorical; sea grass or bare sediment) and individual bird as a random effect.

Table 2
Mixed-effect model results for probe rate: test statistics and parameter estimations

	Estimate	SE	t	P
Probe rate (per s)				
Fixed effects				
Intercept	15.277	1.401	10.882	<0.0001
Prey depth (1, 2, 3 cm)	−4.977	0.397	−12.548	<0.0001
Habitat (sea grass)	1.562	0.916	1.705	0.1
Prey density	−0.032	0.049	−0.654	0.512
Random effects				
Individual bird	1.062	(SD)		
Residual	1.946	(SD)		

Mixed-effect model of probe rate, with fixed effects prey depth (continuous), prey density (continuous), habitat (categorical; sea grass or bare sediment) and individual bird as a random effect.

searching efficiency based on a touch model did not differ from the observations when prey were buried at greater depths (Fig. 1a; at 1 cm: difference$_{observed-predicted}$ = −3.78 cm^2/s, t_{23} = −5.31, $P < 0.001$; at 2 cm: −0.16 cm^2/s, t_{22} = −1.53, $P = 0.14$; at 3 cm: 0.11 cm^2/s, t_{24} = −0.84, $P = 0.41$; observed estimates: bias-corrected back-transformed; Sprugel, 1983). This implies that red knots were unable to use remote detection when foraging in sea grass.

The Physical Model

The physical model shows that the pressure patterns produced by the probing knot's bill, located at the interface between air and sediment, and the flow through the pores, driven by pressure differences, are influenced by the presence of a spherical shell deeper in the sediment (see Fig. 2a,b for details). The pressure pattern induced by the presence of the shell is defined by subtracting the response of the initial pulse with the spherical shell in place from that without it. It is this difference that we argue is sensed and informs the knot about the presence of a prey, at some radial distance and direction (Fig. 2b). In sea grass, however, the pressure field is changed (see Fig. 2c). When we again subtract the response pulse with the spherical shell in place from that without it, we see that the pressure field no longer reveals the presence of the shell (Fig. 2d).

DISCUSSION

Searching efficiency of red knots foraging in sea grass was much lower than when foraging in bare sediment, especially for prey buried at greater depths, and was better explained by the touch model than by remote detection (Fig. 1a). The present estimates of searching efficiency on bare sediment were similar to previous estimates (5.8–26.2 cm^2/s; van Gils & Piersma, 2004; Piersma et al., 1995). Nevertheless, we found a small negative effect of depth in bare sediment, an effect not found by Piersma et al. (1995). However, as searching efficiencies in bare sediment were higher than predicted by the touch model, and were quantitatively in line with previous estimates, we conclude that red knots used remote prey detection in bare sediment at all depths (Fig. 1a). Our finding of the low searching efficiencies (even lower than in the direct touch model) at the shallower prey depths (Fig. 1a) is probably the result of invisible prey rejections below ground. Searching efficiency is derived from number of prey encountered, so that when prey are detected but rejected below ground without being noticed by the observer, searching efficiency will be underestimated (van Gils et al., 2015; Piersma et al., 1995; Wanink & Zwarts, 1985). This bias is likely to become more systematic at high prey densities or at shallow depths when prey are more easily found (Wanink & Zwarts, 1985; T. Piersma, personal observation).

Handling time increased with prey depth and was higher in sea grass, an effect also found by Piersma et al. (1995). In addition, handling time increased more strongly with depth in sea grass which may well be caused by the difficulty for red knots of pulling a prey out of a dense network of rhizomes. The average handling time was 0.92 ± 0.04 s, which is close to a mean handling time of 0.7 s measured in the field (van Gils et al., 2015).

Why do red knots lose their ability to remotely detect hard-shelled prey when foraging in sea grass? The outcome of the physical model shows that when the spherical shell is situated within a layer of rhizomes, the permeability of this substrate is reduced; the pressure field is changed at the interface between the sediment and the rhizomes (Fig. 2c). This overwhelms the much weaker pressure difference due to the reflection by the shell and obscures the directional prey information. Therefore, red knots can no longer rely on their remote detection to encounter the hard-shelled prey 'hidden' by the rhizome layer. It also falsely suggests the presence of a prey item at a certain distance right below the bill tip. This indicates that, relative to the vertical, the angular spread of successful deep probes of knots feeding over a rhizome mat should be significantly less than that over a mud layer without a rhizome mat, a hypothesis that deserves testing (see a detailed discussion on the sensitivity of the pressure gradient to the permeability in Appendix 2). All of the pressure differences, of course, also depend on the actual change in permeability due to the rhizome mat, on the location of that layer and on its depth (here assumed to be of infinite extent). But the dramatic change in the pressure difference that we see because of the rhizome layer (compare Fig. 2b,d) will not depend too much on these details.
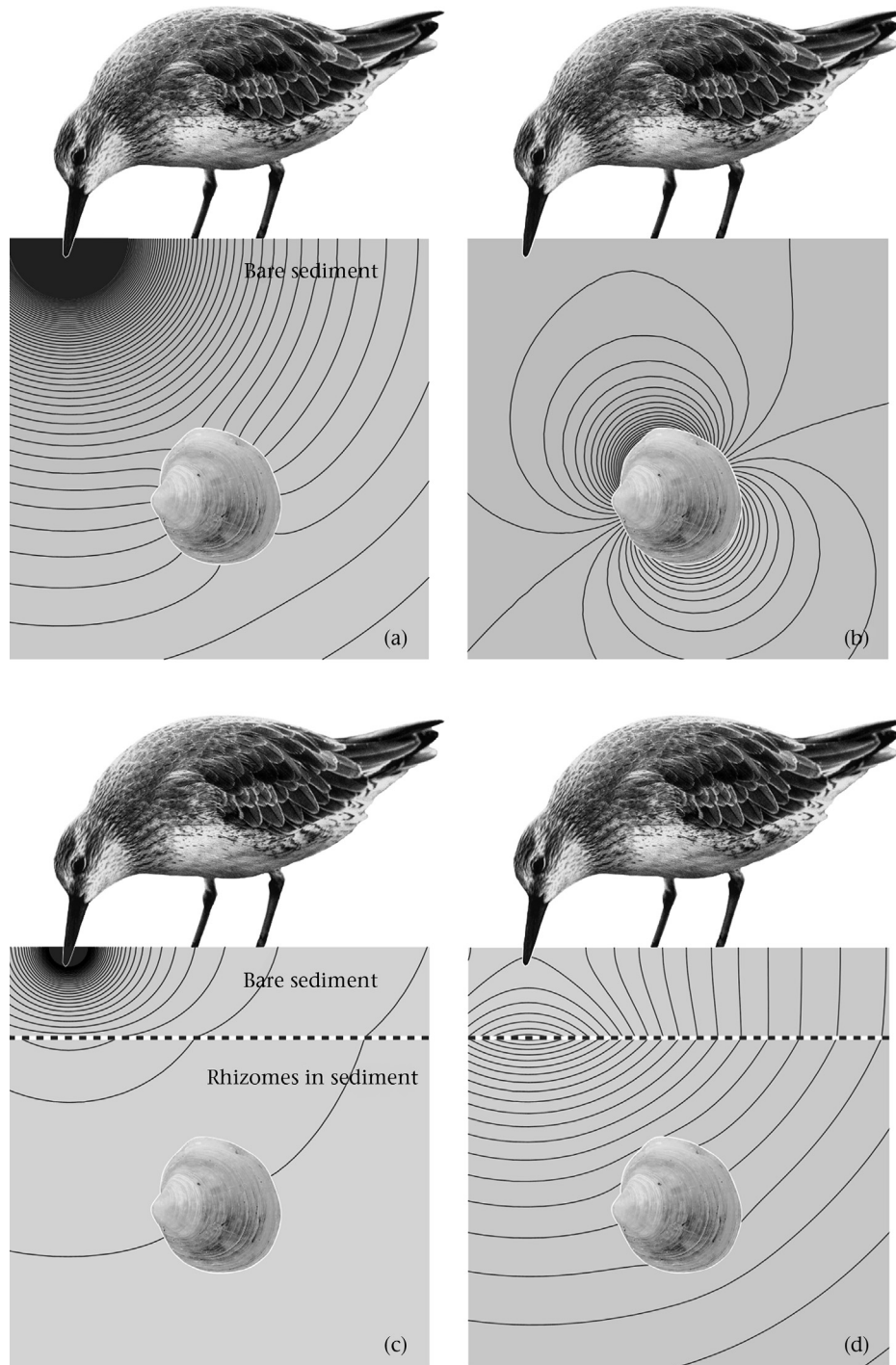
Figure 2. (a) The pressure field build-up by the bill of the knot in bare wet sediment of a hypothetical mudflat. The imposed pressure gradient is displayed by a spherically symmetric radial decay decreasing from high pressure (densely packed isobars near bill tip) to low pressure (wider spaced isobars to right). (b) The isobars are obstructed in the vicinity of the shell, and the disturbance pressure field (shown here) is sensed and informs the knot about the presence of a prey, in the form of radial distance and direction. (c) When the spherical shell is situated within an infinite rhizome layer (below the interface between bare wet sediment and infinitely deep rhizome layer, dashed line), which reduces the permeability, the rhizome layer changes the apparent strength of the source at the origin. The change in the pressure field at the interface between wet sediment and rhizome layer is visualized by a changing isobar inclination. (d) Here, the pressure difference is nearly symmetric at the bill tip, at the origin, and no longer offers any clues on the direction (or distance) at which the prey can be found (for details see Appendix 2).

Implications for Predictions on Intake Rates and Habitat Use

Insights into nonvisual sensory systems may give tantalizing opportunities to actually predict habitat selection rules and even foraging distributions (Cunningham et al., 2010; van Gils et al., 2006; Piersma, 2011, 2012). In this study, the remote detection ability of red knots was obstructed by sea grass resulting in decreased searching efficiencies, an important parameter to predict intake rates with a functional response. The functional response is a commonly accepted function to predict spatial distributions and habitat use of foragers (van Gils et al., 2015; Piersma et al., 1995; Stephens & Krebs, 1986). However, in bare sediment, where
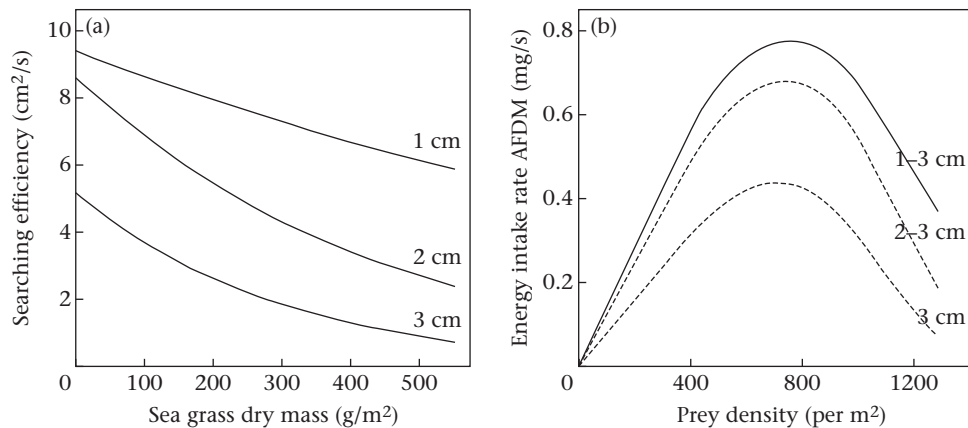
Figure 3. (a) Observed searching efficiency versus sea grass density based on experimental results at different prey depths. (b) The predicted functional responses by red knots, cumulative across all prey depths within the experiments (1–3 cm), and cumulative across the two deepest layers (2–3 cm) and for the deepest layer (3 cm). Depth-specific prey density fractions are from the field. AFDM: ash-free dry mass.

searching efficiency is a constant, red knots obey the assumptions of Holling's type II functional response, implying that intake rate in relation to prey density levels off at high prey densities (this study; Holling, 1959; Piersma et al., 1995). Based on our experimental and physical model results we argue below that in sea grass beds the relation between intake rate and prey density will be dome-shaped (so called type IV functional response; Holling, 1961; Jeschke & Tollrian, 2007), implying that above a certain prey density, the intake rate goes down with increasing prey density.

It is known that sea grass has a positive effect on prey density and abundance (van Gils et al., 2015; Honkoop et al., 2008; Orth, Heck, & van Montfrans, 1984). In Banc d'Arguin, sea grass and lucinid bivalve densities are tightly linked due to their mutualistic relationship (van der Heide et al., 2012). While at first sight the increase in prey density would be an advantage for knots, 'simultaneously' increasing sea grass density leads to decreasing searching efficiency (Fig. 3a). Hence, with an increasing sea grass biomass, the searching efficiency decreases faster than the increase in prey densities, so that the functional response will become dome-shaped, and this goes for all depth distributions (Fig. 3b; see mathematical details in Appendix 3).

Thus, on the Banc d'Arguin, red knots encounter high searching efficiencies at low prey densities in little or no sea grass, and low searching efficiencies with high prey densities in dense sea grass beds. This shows that in sea grass habitats knots may maximize intake rates by feeding on intermediate prey densities and moderately dense sea grass beds (which is indeed what has been found by van Gils et al., 2015). In other words, in this case the functional response may not be a simple function of prey density but also of sea grass density. Note that in herbivores a type IV response is commonly observed, often because digestive quality decreases with increasing biomass (Fryxell, 1991; Heuermann, van Langevelde, van Wieren, & Prins, 2011). However, in predator–prey interactions a type IV functional response has not received much attention. Only a handful of recent studies have shown that density-dependent defences, and nutritional quality of the prey, lead to a decline in intake rate at high prey densities (Bijleveld et al., 2016; Bressendorff & Toft, 2011; Liznarova & Pekar, 2013; Vucic-Pestic, Birkhofer, Rall, Scheu, & Brose, 2010), again suggesting that in many foraging contexts animals should aggregate at intermediate prey densities.

In the Wadden Sea, spatial prediction of foraging red knots was better with than without the refinement of the functional response based on remote detection (Piersma et al., 1995). In sea grass beds,

when sea grass-dependent searching efficiency is not taken into account this may lead to an overestimation of intake rates at high prey densities. The notion of a sea grass-dependent searching efficiency offers a quantitative working hypothesis for future research in diet and habitat preference of red knots foraging on sea grass-covered ecosystems.

References

Ahmedou Salem, M. V., van der Geest, M., Piersma, T., Saoud, S., & van Gils, J. A. (2014). Seasonal changes in mollusc abundance in a tropical intertidal ecosystem, Banc d'Arguin (Mauritania): testing the 'depletion by shorebirds' hypothesis. *Estuarine, Coastal and Shelf Science, 136*, 26–34.

Altenburg, W., Engelmoer, M., Mes, R., & Piersma, T. (1982). *Wintering waders on the Banc d'Arguin, Mauritania. Report of the Netherlands Ornithological Expedition 1980*. Leiden, The Netherlands: Stichting Veth tot steun aan Waddenonderzoek.

Au, W. W. L., Benoit-Bird, K. J., & Kastelein, R. A. (2007). Modeling the detection range of fish by echolocating bottlenose dolphins and harbor porpoises. *Journal of the Acoustical Society of America, 121*(6), 3954–3962.

Bijleveld, A. I., MacCurdy, R. B., Chan, Y., Penning, E., Gabrielson, R. M., Cluderay, J., et al. (2016). [Understanding spatial distributions: negative density-dependence in prey causes predators to trade-off prey quantity with quality] Proceedings of the Royal Society B: Biological Sciences. in press.

Boonman, A. M., Boonman, M., Bretschneider, F., & van de Grind, W. A. (1998). Prey detection in trawling insectivorous bats: duckweed affects hunting behaviour in Daubenton's bat, *Myotis daubentonii. Behavioral Ecology and Sociobiology, 44*(2), 99–107.

Bressendorff, B. B., & Toft, S. (2011). Dome-shaped functional response induced by nutrient imbalance of the prey. *Biology Letters, 7*(4), 517–520.

Cunningham, S. J., Alley, M. R., Castro, I., Potter, M. A., Cunningham, M., & Pyne, M. J. (2010). Bill morphology of Ibises suggests a remote-tactile sensory system for prey detection. *Auk, 127*(2), 308–316.

Cunningham, S., Castro, I., & Alley, M. (2007). A new prey-detection mechanism for kiwi (*Apteryx* spp.) suggests convergent evolution between paleognathous and neognathous birds. *Journal of Anatomy, 211*(4), 493–502.

Cunningham, S. J., Castro, I., & Potter, M. A. (2009). The relative importance of olfaction and remote touch in prey detection by North Island brown kiwis. *Animal Behaviour, 78*(4), 899–905.

de Fouw, J., Kok, E. M. A., Penning, E., van der Heide, T., Piersma, T., & van Gils, J. A. (2016). *[Multiple dimensions of habitat selection: how the combined effects of food density and detectability drive forager distributions].* Unpublished manuscript.

Fryxell, J. M. (1991). Forage quality and aggregation by large herbivores. *American Naturalist, 138*(2), 478–498.

van der Geest, M., van Gils, J. A., van der Meer, J., Olff, H., & Piersma, T. (2011). Suitability of calcein as an *in situ* growth marker in burrowing bivalves. *Journal of Experimental Marine Biology and Ecology, 399*(1), 1–7.

Gerritsen, A. F. C., & Meiboom, A. (1986). The role of touch in prey density estimation by *Calidris alba. Netherlands Journal of Zoology, 36*(4), 530–561.

van Gils, J. A., & Ahmedou Salem, M. V. (2015). Validating the incorporation of ^{13}C and ^{15}N in a shorebird that consumes an isotopically distinct chemosymbiotic bivalve. *PLoS ONE, 10*, e0140221.

van Gils, J. A., van der Geest, M., De Meulenaer, B., Gillis, H., Piersma, T., & Folmer, E. O. (2015). Moving on with foraging theory: incorporating movement decisions into the functional response of a gregarious shorebird. *Journal of Animal Ecology, 84*(2), 554–564.

van Gils, J. A., van der Geest, M., Jansen, E. J., Govers, L. L., de Fouw, J., & Piersma, T. (2012). Trophic cascade induced by molluscivore predator alters pore-water biogeochemistry via competitive release of prey. *Ecology, 93*(5), 1143–1152.

van Gils, J. A., van der Geest, M., Leyrer, J., Oudman, T., Lok, T., Onrust, J., et al. (2013). Toxin constraint explains diet choice, survival and population dynamics in a molluscivore shorebird. *Proceedings of the Royal Society B: Biological Sciences, 280*(1763), 20130861.

van Gils, J. A., & Piersma, T. (2004). Digestively constrained predators evade the cost of interference competition. *Journal of Animal Ecology, 73*(2), 386–398.

van Gils, J. A., Schenk, I. W., Bos, O., & Piersma, T. (2003). Incompletely informed shorebirds that face a digestive constraint maximize net energy gain when exploiting patches. *American Naturalist, 161*(5), 777–793.

van Gils, J. A., Spaans, B., Dekinga, A., & Piersma, T. (2006). Foraging in a tidally structured environment by red knots (*Calidris canutus*): ideal, but not free. *Ecology, 87*(5), 1189–1202.

van der Heide, T., Govers, L. L., de Fouw, J., Olff, H., van der Geest, M., van Katwijk, M. M., et al. (2012). A three-stage symbiosis forms the foundation of sea grass ecosystems. *Science, 336*(6087), 1432–1434.

Heuermann, N., van Langevelde, F., van Wieren, S. E., & Prins, H. H. T. (2011). Increased searching and handling effort in tall swards lead to a Type IV functional response in small grazing herbivores. *Oecologia, 166*(3), 659–669.

Holling, C. S. (1959). Some characteristics of simple types of predation and parasitism. *Canadian Entomologist, 91*(7), 385–398.

Holling, C. S. (1961). Principles of insect predation. *Annual Review of Entomology, 6*, 163–182.

Honkoop, P. J. C., Berghuis, E. M., Holthuijsen, S., Lavaleye, M. S. S., & Piersma, T. (2008). Molluscan assemblages of sea grass-covered and bare intertidal flats on the Banc d'Arguin, Mauritania, in relation to characteristics of sediment and organic matter. *Journal of Sea Research, 60*(4), 235–243.

Hulscher, J. B. (1982). The oystercatcher *Haematopus ostralegus* as a predator of bivalve *Macoma balthica* in the Dutch Wadden Sea. *Ardea, 70*(2), 89–152.

Jeschke, J. M., & Tollrian, R. (2007). Prey swarming: which predators become confused and why? *Animal Behaviour, 74*, 387–393.

Lamb, H. (1932). *Hydrodynamics* (6th ed.). NewYork, NY: Dover.

Larkum, A. W. D., Orth, R. J., & Duarte, C. M. (2006). *Sea grasses: Biology, ecology and conservation.* Dordrecht, The Netherlands: Springer.

van Lent, F., Nienhuis, P. H., & Verschuure, J. M. (1991). Production and biomass of the sea grasses *Zostera noltii* Hornem. and *Cymodecea nodosa* (Ucria) Aschers. at the Banc d'Arguin (Mauritania, NW Africa): a preliminary approach. *Aquatic Botany, 41*(4), 353–367.

Liznarova, E., & Pekar, S. (2013). Dangerous prey is associated with a type 4 functional response in spiders. *Animal Behaviour, 85*(6), 1183–1190.

Madsen, P. T., Kerr, I., & Payne, R. (2004). Echolocation clicks of two free-ranging, oceanic delphinids with different food preferences: false killer whales *Pseudorca crassidens* and Risso's dolphins *Grampus griseus. Journal of Experimental Biology, 207*(11), 1811–1823.

Martin, G. R. (1986). Sensory capacities and the nocturnal habitat of owls (Strigiformes). *Ibis, 128*(2), 266–277.

Miller, L. A., & Surlykke, A. (2001). How some insects detect and avoid being eaten by bats: tactics and countertactics of prey and predator. *BioScience, 51*(7), 570–581.

Nebel, S., Jackson, D. L., & Elner, R. W. (2005). Functional association of bill morphology and foraging behaviour in calidrid sandpipers. *Animal Biology, 55*(3), 235–243.

Orth, R. J., Heck, K. L., & van Montfrans, J. (1984). Faunal communities in sea grass beds: a review of the influence of plant structure and prey characteristics on predator-prey relationships. *Estuaries and Coasts, 7*(4), 339–350.

Ottoni, E. B. (2000). EthoLog 2.2: a tool for the transcription and timing of behavior observation sessions. *Behavior Research Methods Instruments & Computers, 32*(3), 446–449.

Oudman, T., Onrust, J., de Fouw, J., Spaans, B., Piersma, T., & van Gils, J. A. (2014). Digestive capacity and toxicity cause mixed diets in red knots that maximize energy intake rate. *American Naturalist, 183*(5), 650–659.

Piersma, T. (2007). Using the power of comparison to explain habitat use and migration strategies of shorebirds worldwide. *Journal of Ornithology, 148*, S45–S59.

Piersma, T. (2011). From spoonbill to spoon-billed sandpiper: the perceptual dimensions to the niche. *Ibis, 153*(4), 659–661.

Piersma, T. (2012). What is habitat quality? Dissecting a research portfolio on shorebirds. In R. J. Fuller (Ed.), *Birds and habitat: Relationships in changing landscapes* (pp. 383–407). Cambridge, U.K.: Cambridge University Press.

Piersma, T., van Aelst, R., Kurk, K., Berkhoudt, H., & Maas, L. R. M. (1998). A new pressure sensory mechanism for prey detection in birds: the use of principles of seabed dynamics? *Proceedings of the Royal Society B: Biological Sciences, 265*(1404), 1377–1383.

Piersma, T., van Gils, J. A., de Goeij, P., & van der Meer, J. (1995). Hollings functional response model as a tool to link the food-finding mechanism of a probing shorebird with its spatial-distribution. *Journal of Animal Ecology, 64*(4), 493–504.

Piersma, T., de Goeij, P., & Tulp, I. (1993). An evaluation of intertidal feeding habitats from a shorebird perspective–towards relevant comparisons between temperate and tropical mudflats. *Netherlands Journal of Sea Research, 31*(4), 503–512.

R Development Core Team. (2014). *R: A language and environment for statistical computing.* from: http://www.R-project.org/.

Schnitzler, H. U., & Kalko, E. K. V. (2001). Echolocation by insect-eating bats: we define four distinct functional groups of bats and find differences in signal structure that correlate with the typical echolocation tasks faced by each group. *BioScience, 51*(7), 557–569.

Sleath, J. F. A. (1984). *Sea bed mechanics.* New York, NY: Wiley.

Sleep, D. J. H., & Brigham, R. M. (2003). An experimental test of clutter tolerance in bats. *Journal of Mammalogy, 84*(1), 216–224.

Sprugel, D. G. (1983). Correcting for bias in Log-transformed allometric equations. *Ecology, 64*(1), 209–210.

Stephens, D. W., & Krebs, J. R. (1986). *Foraging theory.* Princeton, NJ: Princeton University Press.

Vermaat, J. E., Beijer, J. A. J., Gijlstra, R., Hootsmans, M. J. M., Philippart, C. J. M., Vandenbrink, N. W., et al. (1993). Leaf dynamics and standing stocks of internal *Zostera noltii* Hornem and *Cymodocea nodosa* (Ucria) Ascherson on Banc d' Arguin, Mauritania. *Hydrobiologia, 258*, 59–72.

Vucic-Pestic, O., Birkhofer, K., Rall, B. C., Scheu, S., & Brose, U. (2010). Habitat structure and prey aggregation determine the functional response in a soil predator-prey interaction. *Pedobiologia, 53*(5), 307–312.

Wanink, J., & Zwarts, L. (1985). Does an optimally foraging oystercatcher obey the functional response. *Oecologia, 67*(1), 98–106.

Wilson, C. J., Wilson, P. S., Greene, C. A., & Dunton, K. H. (2013). Sea grass meadows provide an acoustic refuge for estuarine fish. *Marine Ecology Progress Series, 472*, 117–127.

Zwarts, L., & Blomert, A. M. (1992). Why knot *Calidris canutus* take medium-sized *Macoma balthica* when 6 prey species are available. *Marine Ecology Progress Series, 83*(2–3), 113–128.

Appendix 1. Determination of the effective touch area of the prey

To calculate the effective touch area we need to determine the touch area of the prey, because the probability of prey being touched depends on the surface area of the prey, measured in the horizontal plane (Zwarts & Blomert, 1992). The touch area, determined from digital pictures of *Loripes*, is an allometric function of shell length ($N = 27$; see inset of *Loripes* touch area, Fig. A1a) and was analysed with a nonlinear model based on least-squares estimates (function nls; Fig. A1). Red knots probe with a slightly opened bill, apparently to increase the effective touch area (Piersma et al., 1998; Zwarts & Blomert, 1992). Therefore, the touch area is enlarged by the average surface area of the bill tip of the red knot, with t (thickness of bill) $=0.3$ cm and w (width of bill) $= 0.7$ cm (bill parameters taken from Zwarts & Blomert, 1992). The effective touch area is written as: $wt + 2wr + 2tr + \pi r^2$, with r derived from the average touch area from this study based on the allometric function with average prey length of 0.9 cm used in the experiment (see Zwarts & Blomert, 1992 for details). Finally, the effective searching efficiency ('touch model') was calculated by multiplying the effective touch area by the effective probe rate at each depth (1 cm classes; Fig. A1b).

Appendix 2. Physical mechanism of remote touch

Observation and experiments by Piersma et al. (1998) show that knots are able to sense the remote presence of shells (or pebbles), of
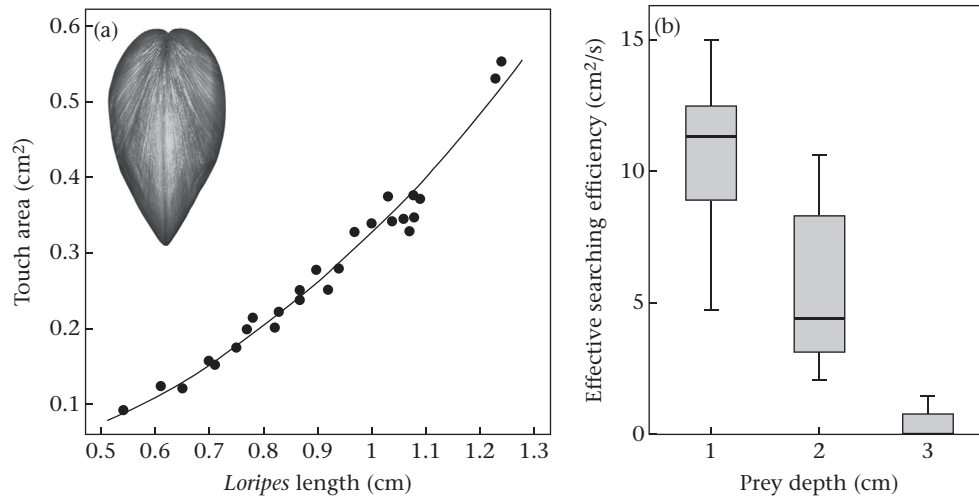
Figure A1. (a) Touch area as a function of shell length: $10^a \times L^b$.($a = -0.486 \pm$ SE 0.006, $t = -84.36$, $P < 0.001$, $b = 2.145 \pm 0.083$, $t = 25.88$, $P < 0.001$). Average shell length L in the experiments was 0.9 cm. (b) Estimated searching efficiency based on the touch model. The horizontal line in each box plot shows the median value, the bottom and top of the box show the 25th and 75th percentiles (middle 50% of the data), respectively, and whiskers show 1.5 times the interquartile range of the data.

some 1 cm diameter, in muddy sand. Knots can sense hard-shelled objects, buried over distances up to their bill length (approximately 3 cm). It is significant that their sensory capability fails in dry sand, in very liquid mud and, what is of particular interest here, when there is a rhizome mat shielding their prey (see main text for description).

Observation also shows that the tip of the knot's bill is (uniformly) covered with many tiny pressure sensors (Herbst corpuscles), whose threshold sensitivity (the minimally detectable pressure perturbation) and response time are unknown. We make a few assumptions concerning the bill that will be convenient in its physical modelling. We assume that the probing depth is very small, so that the probe, in its 'emitting' (forcing) mode, acts as a point source of pressure fluctuations (located at the surface). This is also an accurate description when the emission is produced by a finite-sized spherical object, as long as the same mass flux is affected. For the conical shape of the bill this should be modified at a later stage. During its detection mode, we assume that the bill penetrates to its true depth.

We first address the following questions related to the pressure detection mechanism of probing bills and the specific demands posed on the mud and hydrodynamic environment. (1) What is the role of fluid in the mud, and why does the detection mechanism fail in dry or very liquid circumstances? (2) What is the role of the repetitive character of the probing? (Why is a single probe not sufficient?) (3) What is the role of the rhizome layer in the detection mechanism?

Role of Fluid in the Mud Layer

The probing of the bill will produce pressure variations in the mud. The properties of the medium at hand determine in what way it responds to pressure variations. In dry sandy sediments, for instance, pressure perturbations can, to a large extent, simply be supported by increased or decreased normal stresses of one sand grain upon another, without the necessity of having to yield. In other words, for tiny pressure perturbations, the sand, except in the very vicinity of the bill, acts as a solid. Fluids, on the other hand are unable to support pressure differences and always have to 'yield'. Consequently, they will immediately start to flow, thereby relaxing the pressure difference. Moreover, when forcing is at a liquid surface, the fluid will also respond by means of waves on that surface

that will quickly remove the added energy towards infinity. In a muddy environment, however, there is enough water in the pores to produce a flow through it, while the absence of a free, liquid surface eliminates the ability to remove energy by means of surface wave propagation. The pressure perturbation generated is, in other words, trapped in the forcing location.

The flow through pores is driven by pressure differences. The pores are tiny channels whose sides exert a drag on the flow along them. Indeed, side wall friction is the dominating mechanism which impedes the flow through the pores. The classical description of flow through mud is therefore one in which the pressure gradient is balanced by friction. Because of the complexity of the sand skeleton this is necessarily an empirical relation, known as Darcy's law (e.g. Sleath, 1984):

$$\mathbf{u} = -k\nabla p,$$

where $\mathbf{u} = (u, v, w)$ is the fluid velocity in direction $x = (x, y, z)$ respectively, z pointing upwards, against gravity, p is the pressure, $\nabla = (\partial/\partial x, \partial/\partial y, \partial/\partial z)$ the gradient operator, and k an empirical constant proportional to the mud's permeability (proportional to the porosity of the mud), and inversely proportional to the viscosity of water. Although the pores may contain a substantial amount of air, which will make the aggregate of air and water within the pores susceptible to compression, we adopt the simplistic viewpoint that the pores are entirely filled with water, which is (nearly) incompressible. Hence the fluid is nondivergent:

$$\nabla\cdot\mathbf{u} = 0$$

(Accounting for the slight compressibility of water, or of the water–air mixture, would enable us to describe acoustic waves. For the range of probing frequencies given, however, these waves would have length scales of some hundreds of metres, far outside the range of interest of 5 cm, say.) Incompressibility of the pore water (adopted here) means that pressure variations will instantaneously be felt throughout this domain of interest. The probing bill will bodily displace sand and water and thus will also act as a mass source. This is modelled by introducing a source term at the right-hand side of the last equation. In the approximation that this is a point source this will take the character of a Dirac delta function

$\delta(\mathbf{x})$, a 'distribution' whose integral value only has physical significance representing the mass flux.

Role of Repetitive Probing

Assuming the permeability k to be spatially uniform, the previous two equations, with the addition of a point source, can be combined into a Poisson equation for the pressure:

$$\Delta p = \delta(\mathbf{x})e^{2\pi i f t}, \qquad (1)$$

where the Laplacian operator $\Delta = d^2/dx^2 + d^2/dy^2 + d^2/dz^2$. Note that this only determines a spatial relationship for the pressure. Its time (t) dependence (introduced by the repetitive probing with frequency f) is parametric: $p \propto \exp(2\pi i f t)$. Omitting the time dependence (see below) the Poisson equation, (1), is solved by $p = 1/r$, where $r = (x^2 + y^2 + z^2)^{1/2}$ represents radial distance. The pressure in an infinite medium (for the moment disregarding the upper surface) is thus simply inversely proportional to the distance to the source.

The knot's 'sixth sense' for remote detection of prey (Piersma et al., 1998), employing repetitive, shallow probing, followed by a single deep probe in another direction, apparently uses the build-up of residual pressure near the knot's bill tip. Compaction may be responsible for this pressure build-up. The periodic 'shaking' of muddy sand by the probing action of the bill may explain the continuous increase in residual pore pressure. Each shake may lead to a (locally) more compact rearrangement of sand grains when the stirred-up sand grains fall back under the action of gravity. This process may lead to an associated increase in pore pressure and plays a dominant role, for example, in liquefaction and the formation of quick sand (Sleath, 1984). But the pressure field is not only changing in the vicinity of the bill. The residual (time-averaged) pressure pattern in the vicinity of a nearby shell will be affected as well, and in consequence this will in turn affect the pressure distribution around the bill. The intensity of this spatially modified pressure pattern will increase at each successive cycle of the probing action, revealing the prey's location by making it, in every cycle, more clearly 'visible'.

Response due to a Rhizome Layer with or Without a Shell

At the top of the rhizome layer, situated at depth $z = -d$, the pressure, p, and the vertical velocity, $w = -kdp/dz$, perpendicular to that plane, have to be continuous. The permeability, k, of the lower rhizome layer, k_l, is less than that of the upper mud layer, k_u. This is due to the decrease in the effective porosity of the sediment, and we assume that the rhizome root structure is so small that we can represent its presence in the form of a reduced effective permeability.

We next describe the response due to a localized pressure pulse induced by repetitive probing of a knot's bill, at z=0. We consider three cases: first, the response in the absence of a shell, when a mud layer rests on top of a layer containing a rhizome mat; second, the response to a shell in a mud layer without a rhizome mat, qualitatively discussed in Piersma et al. (1998); third, the response to a shell buried in the lower layer containing the rhizome mat. In the latter case we give particular attention to the pressure gradient sensed at the position of the knot's bill.

Response due to a rhizome layer without a shell

Even in the absence of a prey (or stone) the change in permeability between a mud layer and a layer containing a sea grass root system (rhizome mat) will affect the radial pressure distribution discussed above. Assuming the permeability to be constant within the rhizome layer, the pressure will again be governed by a Laplace equation. Hence the pressure will also be inversely proportional to the radius, but with a reduced 'transmitted' amplitude T. The semipermeable interface between the mud and rhizome layers acts as a partial mirror. Therefore it augments the pressure field in the mud layer, where the knot senses the pressure difference relative to the uninhibited pressure field it knows it has been producing. This augmented field in the mud layer seems to come from a mirror source situated in the rhizome layer at a distance from the interface at $z = -d$ equal to that of the source (the bill), at the surface and the interface. Therefore, the pressure is written as

$$p(x,y,z) = \begin{cases} p_u = \dfrac{1}{r_0} + \dfrac{R}{r_{-1}}, & z \in (-d, 0) \\[2mm] p_l = \dfrac{T}{r_0}, & z < -d \end{cases} \qquad (2)$$

where $r_n \equiv (x^2 + y^2 + (z + Z_n)^2)^{1/2}$, denotes the distance with respect to source ($n = 0$) or images, located at $Z_n = -2nd$ for $n = (1, 2, \ldots)$. At the interface between mud and rhizome layer, $z = -d$, we require continuity of the pressure $p_u = p_l$, (subscripts denoting upper (u) and lower (l) layer, respectively), and also continuity of vertical velocity $k_u dp_u/dz = k_l dp_l/dz$. This determines reflection and transmission coefficients R and T in terms of $k \equiv k_l/k_u < 1$:

$$R = \frac{1-k}{1+k}, T = \frac{2}{1+k}. \qquad (3)$$

The resulting pressure field is displayed in Fig. A2a.

In this computation, the top layer ($z > -d$) is treated as being of infinite extent. Therefore, the normal derivative of the pressure, dp/dz, and hence the vertical velocity, w, do not vanish at the water surface, $z = 0$. Fig. A2a shows a weak inclination of the isobars relative to the vertical. The presence of the water surface, however, leads to a subsequent reflection of our virtual source at $z = -2d$, which creates a new mirror image above the water surface, at $z = 2d$. This mirror source, in turn, will produce a subsequent mirror source in the rhizome layer at $z = -4d$ and so on, ad infinitum, and the pressure field due to this infinite sequence of source and mirror images is given by

$$p(x,y,z) = \begin{cases} p_u = \displaystyle\sum_{n=0}^{\infty}\left(\dfrac{R^n}{r_n} + \dfrac{R^{n+1}}{r_{-(n+1)}}\right), & z \in (-d, 0) \\[3mm] p_l = T\displaystyle\sum_{n=0}^{\infty}\dfrac{R^n}{r_n}, & z < -d \end{cases} \qquad (4)$$

Taking, for example, 50 mirror sources into account, the isobars indeed approach the water surface practically orthogonally (see Fig. A2b). When we subtract the initial pulse, we find the pressure perturbation as sensed by the knot (Fig. A2c), which the knot may take to indicate the presence of a prey straight below its bill.

Perturbation due to a spherical shell

We now consider the impact of a shell (Piersma et al., 1998). For convenience this is assumed to be of spherical shape or radius $a < 1$, located at a radial distance $r = 1$ from the bill tip, at an oblique angle θ from the horizontal. In an infinitely extended mud layer, an appropriate array of image sources and sinks, located within the shell, will be able to generate a pressure and corresponding motion field such that the isobars are everywhere perpendicular, and thus the flow is parallel to the shell's boundary (Lamb, 1932; p. 129; Fig. A3a). We let the source be at the origin and the centre of the shell defines the x, z-plane. The residual pressure field is then most easily expressed in
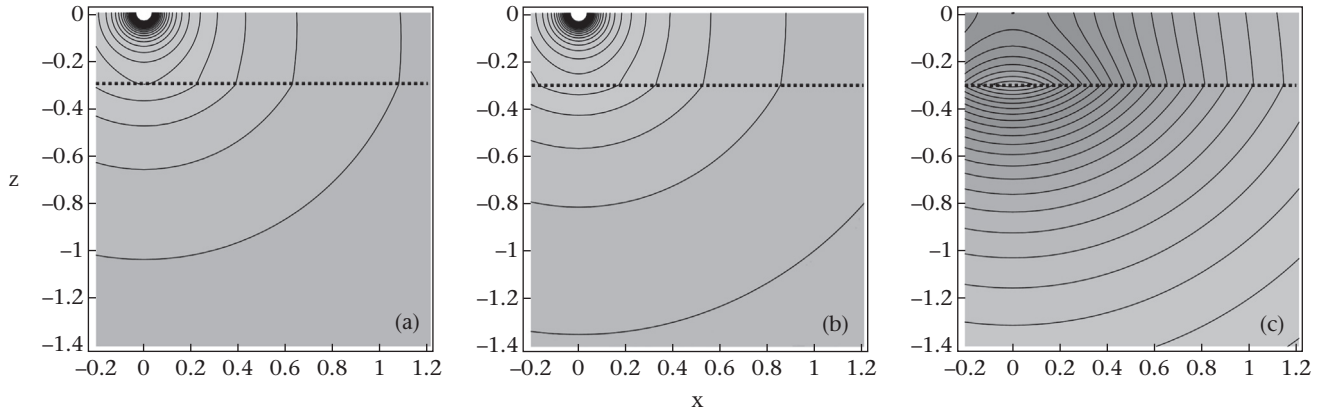
Figure A2. Rhizome layer without a shell. Pressure distribution, $p(x, z)$, for $k = 0.25$ taking in the summation (a) only the $n = 0$ term into account, or (b) up to $n = 50$. The top of the rhizome layer is indicated by a dashed line. (c) Pressure perturbation, $p'(x, z) \equiv p - 1/r$, after eliminating the forced pulse at the source.

a coordinate system in which the x, z-coordinates, rotated to ξ, ζ-co-ordinates, with $\xi = -xs + zc$, $\zeta = xc + zs$, and $(s, c) \equiv (\sin\theta, \cos\theta)$, are such that the line connecting bill tip and prey is now defined as the new horizontal ξ-axis, and the line perpendicular to this as the new vertical ζ-axis. Then the residual pressure reads

$$p(x, y, z) = \frac{1}{r} + \frac{a}{\sqrt{(1 - a^2 - \zeta)^2 + \rho^2}} + \frac{1}{a}\left[\sinh^{-1}\left(\frac{1 - a^2 - \zeta}{\rho}\right)\right.$$
$$\left. - \sinh^{-1}\left(\frac{1 - \zeta}{\rho}\right)\right],$$

where $\rho = (\xi^2 + y^2)^{1/2}$ is a horizontal radial coordinate. Subsequent figures show the $y = 0$ plane only (the plane containing bill tip and prey), in which the response is strongest. When we subtract the initial pulse, we find, however, that the isobars of the perturbation pressure field are not perpendicular to the water surface, $z = 0$, suggesting a flow through the surface (Fig. A3b) but this does not happen since the water surface is impenetrable. The surface acts as a reflector leading to another change in the pressure field. This is produced by a mirror image of the virtual sources produced by the shell. Adding this contribution, the isobars are correctly perpendicular to the water surface (Fig. A3c), but at the bill tip, at the origin, $(x, z) = (0, 0)$, this difference is sensed and informs the knot about the presence of a prey at $\theta = 60°$ relative to the horizontal, at a radial distance $r = 1$. Note that these image sources (located above the water surface) would require another perturbation pressure field in the vicinity of the shell, as the flow induced by that

field would equally need to avoid penetrating the shell. In theory, an infinite sequence of virtual sources within the shell and above the water surface would be needed to exactly satisfy the impenetrability at shell and water surfaces. In practice, here and in what follows, we truncate this sequence after a few terms. When the shell is buried in a half-infinite rhizome layer of permeability $k = 0.25$ (leading to a reflection coefficient, $R = 0.6$) below a mud layer of depth $d = 0.3$, the rhizome mat changes the apparent strength of the source at the origin by a factor $T = 1 - R^2$. The change in the pressure field at the interface between mud and rhizome layer is clearly visible in a changing isobar inclination (Fig. A4a). Subtracting the influence of the source (Fig. A4b) shows that the pressure field in the mud layer no longer reveals the presence of the shell, even if we take the mirroring aspect of the surface into account (Fig. A4c). In both cases, the pressure difference is very nearly symmetric at the bill tip, at the origin $x = 0$, and no longer offers any clues on the direction (or distance) at which the prey can be found (compare Fig. A4c with Fig. A3c). In fact, while not exactly symmetric, it is clear that the pressure difference $p' = p - r^{-1}$ between the induced (p) and the imposed pressure (r^{-1}), the difference sensed by the knot, is dominated by the direct reflection due to the presence of the rhizome layer. This overwhelms the much weaker pressure difference due to the reflection by the shell and obscures the directional prey information.
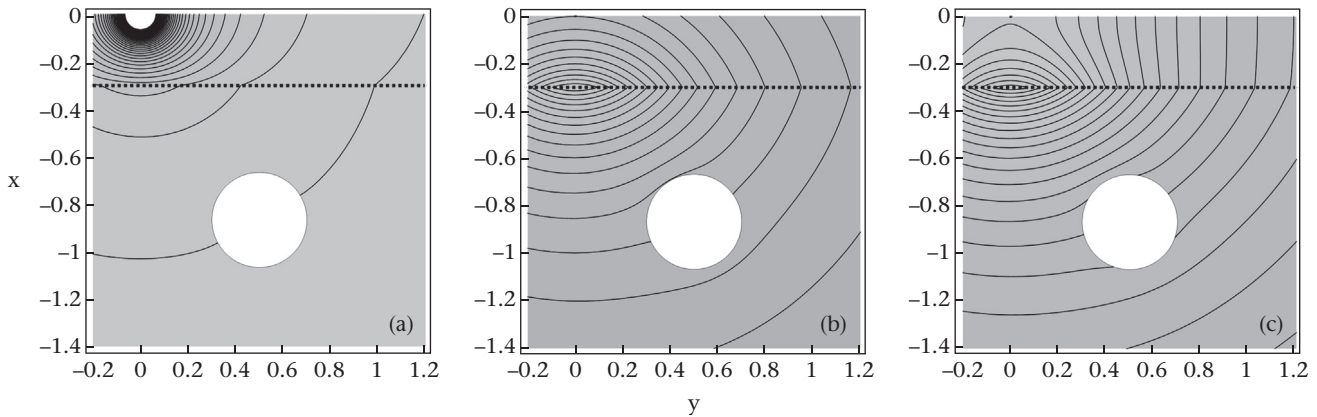
Perturbation pressure gradient

The pressure difference below the top layer of depth d, of course, also depends on the actual change in permeability, k, due to a
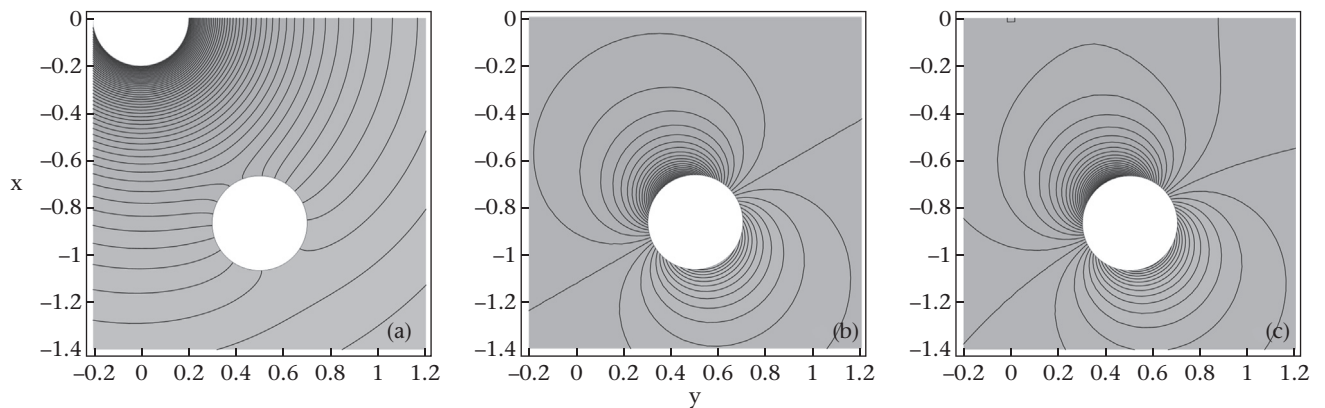
Figure A3. Shell without rhizome layer. (a) Pressure distribution, $p(X, z)$, due to shell in infinitely deep mud layer without rhizomes. (b) Perturbation pressure, $p'(X, z)$ without the source. (c) As (b), but with reflecting water surface.

Figure A4. Shell within a rhizome layer. (a) Pressure distribution, $p(X, z)$, due to shell in infinitely deep rhizome layer located below mud layer. The interface between the layers is indicated by a dashed line. (b) Perturbation pressure $p'(X, z)$ without the source. (c) As (b), but with reflecting water surface.

rhizome mat below, on shell size, a, and on shell angle, θ, relative to the horizontal. (We here assume the rhizome mat to be of semi-infinite extent.) The strength of the pressure gradient as sensed by the knot's bill is estimated by taking only the influence of the rhizome layer and of a shell into account. Thus we discard the subsequent contribution consisting of mirror images due to the presence of the surface. The reason to do so is that the vertical component of the pressure gradient (proportional to the vertical velocity) vanishes at the surface. Since the knot's bill penetrates the mud layer over a few millimetres, the knot also senses this difference below the surface, where this component is not annihilated. In this way, the pressure gradient at the origin,$(x, y) = (0, 0)$, affected by the sea grass roots and a shell, contains, apart from its magnitude, directional information, ϕ, which can be computed analytically. It is given by

$$-\nabla p' \equiv |\nabla p'|(\cos \phi, \sin \phi) = \left(1 - R^2\right)\frac{a^3}{\left(1 - a^2\right)^2}(\cos \theta, \sin \theta)$$
$$+ \left(0, \frac{R}{4d^2}\right).$$

Without a rhizome layer, the permeability ratio $k = 1$, and thus there is no reflection, $R = 0$, and the pressure gradient decreases with decreasing shell size, a. In the vertical plane this points towards the shell position, $\phi = \theta$. With a rhizome layer, but without a shell ($a = 0$), the perturbation pressure gradient points simply

downwards, towards the image source. This may falsely suggest the presence of a shell at a depth $2d$, twice the thickness of the sediment layer on top. For a single depth ($d = 0.3$) and shell diameter ($a = 0.2$), the magnitude $|\nabla p'|$ and direction ϕ, relative to the horizontal, are displayed in Fig. A5a,b. The figure reveals that even under a small 4% drop of permeability in the lower rhizome layer, the perturbation pressure gradient magnitude increases by a factor of 10 (see the left side of Fig. A5a). Obviously, the contribution to the perturbation pressure by the shell is dwarfed by that due to the virtual image source. Most significantly, the angular information on the position of the shell is almost lost, since $\phi \approx 90°$ for any shell direction θ (meaning the knot believes the prey to be buried vertically below the bill). This sensitive dependence on permeability remains present for other surface layer depths, d, and shell diameters, a.

Appendix 3. Functional response

To investigate how searching efficiency affects intake rates (IR) of knots, we integrated the sea grass density-dependent searching efficiency into the type II functional response where h is the constant handling time of the prey (s), a is the constant searching efficiency (m²/s) and D is the prey density (no./m²):

$$IR = \frac{aD}{1 + aDh}$$
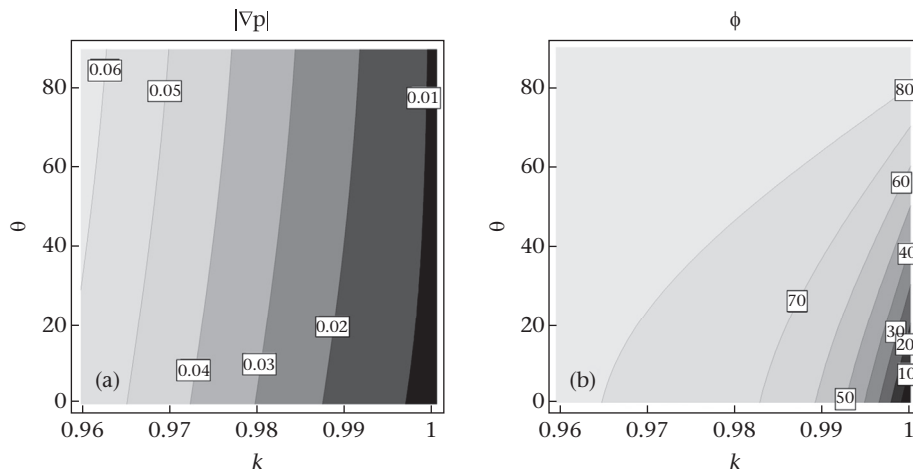
Figure A5. Perturbation pressure gradient sensed at the bill tip ($x = (0, 0, 0)$): (a) magnitude, $|\nabla p|$, (dimensionless units and colours) and (b) direction, ϕ, (labelled contours in degrees and colour) as a function of shell angle to the horizontal, θ, and of permeability ratio, k.

Because searching efficiency is negatively dependent on sea grass density (Fig. 3a) and prey density increases with sea grass density, we introduced a dynamic searching efficiency $A(S)$ that is negatively related to sea grass density S:

$$IR = \frac{A(S)D(S)}{1 + A(S)D(S)h}$$

We described the relation between searching efficiency and prey density by the exponential function $A(S) = A(S=0)\ e^{-cS}$, where the constant c and $A(S=0)$ (the searching efficiency on bare sediment) are fitted to the results of this study. Because the detectability of the prey is depth dependent, all parameters were estimated for all three depth classes separately by a nonlinear model based on least-squares estimates (function nls in R, Fig. 3a; R Development Core Team, 2014). The relationship between prey density and sea grass biomass was recently quantified as non-linearly dependent on sea grass ($D(S) = 256.6\ S^{0.24}$, de Fouw et al., 2016). We use depth-specific prey density fractions from the field (based on Piersma et al., 1993) and length specific energy content of *Loripes* (van Gils et al., 2012). The estimated amount of energy gained based on the functional response becomes dome-shaped and the effect becomes stronger with prey depth (Fig. 3b).